Constraining spectral models of a terrestrial gamma-ray flash from a terrestrial electron beam observation by the Atmosphere-Space Interactions Monitor

D. Sarria[1], N. Østgaard[1], P. Kochkin[1], N. Lehtinen[1], A. Mezentsev[1], M. Marisaldi[1], A. Lindanger[1], C. Maiorana[1], B. E. Carlson[1,2], T. Neubert[3], V. Reglero[4], K. Ullaland[1], S.Yang[1], G. Genov[1], B. H. Qureshi[1], C. Budtz-Jørgensen[3], I. Kuvvetli[3], F. Christiansen[3], O. Chanrion[3], J. Navarro-González[4], P. Connel[4], C. Eyles[4]

[1]Birkeland Centre for Space Science, University of Bergen, Bergen, Norway

[2]Carthage College, Kenosha, Wisconsin, United States

[3]National Space Institute, Technical University of Denmark, Lyngby, Denmark

[4]University of Valencia, Valencia, Spain

Key Points:

- Observation of a Terrestrial Electron Beam with a spectrum resolved down to 50 keV

- A method to constrain the energy spectrum of the source TGF based on the detection of the associated TEB is presented

- Only TGFs originating from fully-developed RREA models can explain the observation

Corresponding author: D. Sarria, `david.sarria@uib.no`

Abstract

Terrestrial Gamma-ray Flashes (TGFs) are short flashes of high energy photons, produced by thunderstorms. When interacting with the atmosphere, they produce relativistic electrons and positrons, and a part gets bounded to geomagnetic field lines and travels large distances in space. This phenomenon is called a Terrestrial Electron Beam (TEB). The Atmosphere-Space Interactions Monitor (ASIM) mounted on-board the International Space Station detected a new TEB event on March 24, 2019, originating from a tropical cyclone Johanina. Using ASIM's low energy detector, the TEB energy spectrum is resolved down to 50 keV. We provide a new method to contrain the TGF source spectrum based on the detected TEB spectrum. Applied to this event, it shows that only fully developed RREA spectrums are compatible with the observation. More specifically, assuming a TGF spectrum $\propto E^{-1} \exp(-E/\epsilon)$, the compatible models have $\epsilon \geq 6.5$ MeV. We could not exclude models with ϵ of 8 and 10 MeV.

Plain Language Summary

Terrestrial Gamma-ray Flashes (TGF), originating from thunderstorms, are the highest energy natural particle acceleration phenomena occurring on Earth. The production mechanism of TGFs is not very well understood. When interacting with the atmosphere, TGFs produce secondary electrons and positrons, and a part gets bounded to Earth's magnetic field lines, and travels large distances in space. They can be detected by instruments on-board satellites located at the right place (in a window of about 40 km) at the right time (in a window of a few milliseconds). This phenomenon is called a Terrestrial Electron Beam (TEB). By detecting the TEB, we can retrieve information about the TGF that produced it. In this article we present the first TEB originating from a tropical cyclone, and with the lowest energies ever recorded (down to 50 keV). We also provide a new method to infer properties of the energy distribution of the TGF (producing the TEB) based on the energy spectrum of the TEB. Applied to this event, it shows that only TGF energy spectrums among the most energetic that were proposed are compatible, and we cannot exclude even more energetic events.

1 Introduction

Terrestrial Gamma-ray Flashes (TGFs) are short bursts of high energy (< 40 MeV) photons, produced during thunderstorms. A review of TGFs theory and observations is presented by Dwyer et al. (2012). TGFs were first detected using the BATSE experiment on-board the CGRO spacecraft (Fishman et al., 1994). Later, TGFs were recorded by the satellites RHESSI (Smith et al., 2005), AGILE (Marisaldi et al., 2014), Fermi (Briggs et al., 2010; Roberts et al., 2018), BeppoSAX (Ursi et al., 2017) and the Atmosphere-Space Interactions Monitor (ASIM) (Neubert et al., 2019). ASIM was successfully launched and docked to the International Space Station in April 2018, and started science operations since June 2018. The first results from ASIM were presented by Østgaard et al. (2019); Sarria et al. (2019); Neubert et al. (2020).

When referring to "electrons beams" in the context of TGFs, one can think of two different objects. The first is associated with the production process of the TGF. This production process takes place, at least for TGF detectable from space, between $\approx$10 and $\approx$15 km altitude. This first type of "electron beam" consists of the Relativistic Runaway Electron Avalanche (RREA) producing the TGF's high energy photons. This RREA is not detectable from space since it is is impossible for it to go through the atmosphere layer. The second type of "electron beam" is called "terrestrial electron beam" (TEB) and is produced higher in the atmosphere by the TGF's photons, though the processes of Compton Scattering and electron-positron pair production. Since electron-positron pair production is involved, TEBs are composed of a fraction of positrons, typically 10 % to 30 % (see Briggs et al. (2011), table 1). A TEB is bound ("beamed") around the magnetic field line intercepting the source TGF's geographical location (Dwyer et al., 2008; Cohen et al., 2010; Sarria et al., 2015). Most electrons and positrons forming TEBs are produced above 40 km altitude, where the air collision frequency of the electrons (and positrons) is comparable to their gyration frequency around geomagnetic field lines. TEBs propagate in space and travel large distances in the magnetosphere. TEBs were first reported from measurements of the CGRO spacecraft (Dwyer et al., 2008). Later, they were detected by Fermi (Briggs et al., 2011), BeppoSAX (Ursi et al., 2017), AGILE (Lindanger et al., 2020) and ASIM (Sarria et al., 2019). RHESSI probably detected one or two TEB event(s), but it has not been 100% confirmed yet (Smith et al., 2006; Gjesteland, 2012). In general, TEBs are detected much less often than TGF (e.g. Fermi has a few thousand TGFs and about 30 TEBs) because the detector must be located inside a narrow win-

81   dow (less than a few tens of kilometers) along the right geomagnetic field line (intercept-

82   ing the TGF source position), and they last only a few milliseconds.

83   One of the reasons of studing TEBs is to retrieve information about the TGFs that

84   produced them. Briggs et al. (2011) constrained the positron fraction to be between 10

85   and 34%, based on 3 events. Positrons fractions are linked to the spectral shape of the

86   source TGF, as photons with harder specturms will do more pair production. In Sarria

87   et al. (2019), the beaming of the source TGF was constrained and found between 20.6^o

88   and 29.8^o (Gaussian angular distribution) or 30.6^o and 41.9^o (isotropic within cone an-

89   gular distribution, half angle). Another reason to study TEBs is that they may have an

90   impact on the inner Van Allen radiation belt, that has not been quantified yet (to our

91   knowledge). Even if it is an important question, it is not the subject of the present pa-

92   per.

93   One of the most important question regarding TGFs is their production mechanism.

94   Two main models are proposed to explain the production of TGFs, and in both, the TGF's

95   photons are produced by high energy electrons through the bremsstrahlung process. In

96   both cases, the high energy electrons form a Relativistic Runaway Electron Avalanche

97   (RREA) (Wilson, 1924; Gurevich et al., 1992). In the first model, a large scale electric

98   fields within thunderclouds is considered. This requires the presence of initial high en-

99   ergy seed electrons, that may be provided by cosmic-ray secondaries or background ra-

100   diation. The background electric field is strong enough to produce RREA avalanches,

101   but the RREA mechanism alone is not enough to produce bright enough TGFs (i.e. de-

102   tectable from space, therefore with more than 10^{16} photons at source), and a x-ray and

103   positron feedback mechanism is required ("relativistic feedback"); only possible if large

104   potentials are available (Dwyer et al., 2003; Babich et al., 2005; Dwyer, 2012; Skeltved

105   et al., 2014). This mechanism will produce a discharge of the thundercloud, that is of

106   different nature than usual lightning discharges. The resulting high-energy photon spec-

107   trum given by this model can only be a fully-developed RREA. The development of a

108   RREA process can be characterized by the number of avalanche lengths that were achieved

109   (that depends on the extend and magnitude of the available potential). A fully-developed

110   RREA spectrum will appear if at least 6 avalanches lengths have been achieved. Another

111   variant of this model uses a lightning leader to push the background (large scale) field

112   above the threshold to trigger the relativistic feedback mechanism.

The second model of TGF production requires a propagating lightning leader. It is sometimes referred as the "leader-streamer" model. It considers that initial seed electrons are produced by the cold runaway mechanism (Gurevich, 1961), happening in the streamer phase or in the leader phase (Moss et al., 2006; Dwyer, 2008; Celestin & Pasko, 2011; Chanrion et al., 2014; Kohn & Ebert, 2015). These energetic seed electrons follow a specific distribution and a fraction of them are then accelerated and multiplied by a larger scale electric field, producing a RREA. The larger scale electric field can be the field induced by the leader and/or a large scale (background) field in the thunderstorm. In principle, leader-based TGF production models do not exclude the possibility of relativistic feedback, that could be more or less important. A parameter that impacts the energy spectrum of emitted photons the most is the potential drop in the leader tip region that is available for the acceleration of energetic electrons. Resulting TGF energy spectrums for several leader potential drops are presented in Celestin et al. (2015), figure 3. They actually correspond to a more or less developed RREA process. Celestin et al. (2012) also showed that energy spectrums harder than this characteristic fully-developed RREA spectrum could be achieved by involving non-equilibrium acceleration of electrons. One significant advantage of leader-based TGF models is that they propose an unified approach to explain TGF's X/gamma-ray production, as well as x-ray (i.e. softer) emissions from lightning propagating leaders, that were observed from ground, balloons and aircraft (Dwyer et al., 2003, 2004, 2005, 2011). Mailyan et al. (2019) presented the first study that confronted leader models to TGFs recorded by the Fermi space telescope, with tested potential drops ≤ 200 MV. They found that lightning leader models with potentials of 200 MV and tilted beams gave the best fit to the data in most of the analyzed TGF events. However, the range of compatible models is found to be quite wide.

In this article, we report the second TEB event detected by ASIM on 24 March 2019. Compared to the previous event (presented in Sarria et al. (2019)), data from the two detectors are available: the pixelated Low-Energy detector (50-400 keV) and the High Energy Detector (400 keV-30 MeV), that permits an unprecedented spectral analysis of a TEB event. In section 2, we present the instruments that were used. In section 3 we present the event. In section 4 we present the methods and models we use for the spectral analysis. In section 5 we show the results of the analysis. We conclude in section 6.

2 Instruments

The ASIM payload (Neubert et al., 2019) consists of two main instruments, the Modular X- and Gamma-ray Sensor (MXGS) (Østgaard et al., 2019) and the Modular Multispectral Imaging Array (MMIA) (Chanrion et al., 2019). ASIM is mounted on the International Space Station (ISS) orbiting the Earth at about 400 kilometers altitude with an inclination of 51.6^o. MXGS consists of two detectors for detecting X- and gamma-rays. The MXGS Low-Energy Detector (LED) is layer of 16384 pixels of Cadmium-Zink-Telluride (CZT) detector crystals, sensitive to photons with energies from 50 keV to about 400 keV. The MXGS High Energy Detector (HED) comprises 12 Bismuth-Germanium-Oxide (BGO) detector modules coupled to photomultiplier tubes (PMT), sensitive in the energy range of 400 keV to about 40 MeV.

GLD360 (VAISALA) is a network of ground-based lightning sensors (1 kHz-350 kHz) detecting both Cloud-to-Groung and Intra-Cloud lightning with a median location accuracy of 250 meters. The GLD360 sensors use a combination of magnetic direction finding and time-of-arrival calculations (from 4 stations or more) to geolocate the lightning source (see acknowledgments for more details).

We also present data provided by the Meteosat-11 geostationary satellite, that provides regular scans of cloud coverage at several wavelengths (used data comes from band 4, at 3.9 μm, with a 3 km spatial resolution). See acknowledgments for more information.

3 Observation

Figure 1 shows a map of the event together with Satellite imagery that was provided by the geostationary satellite Meteosat-11. The ASIM trigger UTC time is 2019-Mar-24 00:31:53.135444 and the ISS was located at latitude of $\phi = 0.157^o$, longitude of $\lambda = 55.301^o$ and altitude of $h = 408.6$ km, that is above the Indian ocean, close to Madagascar. The ASIM clock has a 30 ms absolute timing uncertainty with respect to GPS UTC time. A VAISALA (GLD360) discharge event with a UTC time of 2019-03-24 00:31:53.134000 ($\Delta t = 1.44$ ms) was found very close to the southern magnetic line footpoint (at 45 km altitude) intercepting the ISS position : [$\phi_{GLD360} = -7.049^o$, $\lambda_{GLD360} = 55.912^o$] and [$\phi_{mag,s} = -7.007^o$, $\lambda_{mag,s} = 55.923^o$] that gives $\Delta r = 4.82$ km. Note that the GLD360 location uncertainty is about 20 km, and the uncertainty in the ISS

175 position is of the same order. The northern magnetic field line footpoint is located at

176 $[\phi_{mag,n} = 20.524^o, \lambda_{mag,n} = 55.099^o]$, but no lightning activity was observed close to

177 it.

178 From satellite imagery (figure 1), it appears that the southern magnetic field line

179 footpoint is located in the rainbands a tropical cyclone, named "Joaninha". It is the first

180 time that the detection of a TEB associated to a TGF produced in a cyclone is reported.

181 Figure 2.a shows the recorded lightcurves for LED and HED, as well as a model-

182 ing result. The latter is obtained using what will be referred as the "consensus model",

183 that assumes a source TGF located at the southern magnetic footpoint, at 12 km alti-

184 tude, with an angular distribution following a Gaussian distribution with $\sigma_\theta = 20^o$ (cen-

185 tered on zenith), and with an energy spectrum $\propto\ E^{-1}\exp(-E/7.3\ \text{MeV})$ (maximum

186 energy set to 40 MeV). More information about the modeling is presented in the next

187 section. The consensus model gives a very good fit to the data (see figure label). Fig-

188 ure 2.b shows the spectra recorded by the MXGS instrument for LED and HED. There

189 is a total of 168 counts in HED and 307 counts in LED. The error bars are 1-σ ($\approx$68 %

190 interval) assuming Poisson statistics on the count values given by the model. The spec-

191 trum shows a strong line at 511 keV, that is expected because the electron beams con-

192 tains a significant fraction of positrons. The consensus model gives a very good fit to the

193 spectral data as well (see figure label), and a positron to electron ratio of 16.1 %. This

194 value is comparable to previous results (Briggs et al., 2011).

195 ## 4 Method to constrain the source TGF spectrum

196 As presented in the introduction, for any considered TGF production scenario, the

197 spectral shape for the TGF is governed by the RREA process that produces high-energy

198 photons through the bremsstrahlung process. A RREA can be more or less developed

199 depending on how much avalanches lengths have been achieved, that depends on the avail-

200 able potential (in the leader and/or background electric field) and the extend of the elec-

201 tric field(s). When the RREA process is close to being fully developed, the resulting TGF

202 photon energy spectrum can be well approximated with equation 1:

$$f(E) \propto E^{-1}\exp\left(-E/\epsilon\right), \text{with } E < E_m \tag{1}$$

Where E is the energy, ϵ is a cut-off energy and E_m is the maximum allowed energy. TGF energy spectrums from fully-developed RREA are excepted to have $\epsilon \geq 5$ MeV (Dwyer, 2012; Skeltved et al., 2014; Sarria et al., 2018). Typical TGFs spectrums used in the literature have $\epsilon = 6.5$ to 7.3 MeV, with E_m of 30 to 40 MeV. TGF production models based on a propagating lightning leader can, in theory, produce bright TGFs (i.e. detectable from space, therefore with more than 10^{16} photons at source) but that shows a partially developed RREA spectrum. This is because, for these models, typically 10^{12} (or more) energetic electrons are initially provided by the cold runaway mechanism. Leader models with potential drops as low as ≈ 160 MV could potentially produce bright TGFs (see Celestin et al. (2015), table 1). By "potential drop", it is meant the potential difference between the tip of the lightning leader and the ambient potential.

Equation 1 can fit a fully-developed RREA (using $\epsilon \geq 5$ MeV, $E_m = 40$ MeV), as well as partially developped RREA energy spectrums resulting from leader models. The leader 300 MV model from Celestin et al. (2015) (figure 3) can be fit by equation 1 with $\epsilon = 4.7$ MeV and $E_m = 30$ MeV as it is close to a fully-developed RREA spectrum. The 160 MV leader model can be fit by equation 1 using $\epsilon = 4.3$ MeV and $E_m = 20$ MeV. In the cases of potential drops of 160 and 300 MV, the initial electron's positions are set at 2 meter and 3.5 meter from the leader tip, respectively, because of the shielding of the electric field (Skeltved et al., 2017). The corresponding effective electric potential drops (i.e. that the energetic electrons can use) are respectively 28 MV, and 53 MV (Celestin et al., 2015).

In addition to the 160 and 300 MV leader spectrums, we chosed to test spectrums with ϵ equal to 6.5 MeV, 7.3 MeV, 8 MeV and 10 MeV (all using $E_m = 40$ MeV). The first two values correspond to values used in the literature (Dwyer et al., 2012; Bowers et al., 2017; Sarria et al., 2018; Xu et al., 2019). After looking at the preliminary results using these two values, we decided to add $\epsilon = 8$ MeV and $\epsilon = 10$ MeV. These last two values were primarily added on an ad hoc basis, but a physical justification is that, in theory, non-uniform electric fields in leader models can also produce TGF spectrums harder than typical fully-developed RREA if non-uniform electric fields are involved (Celestin et al., 2012). We decided not to go above $\epsilon = 10$ MeV and $E_m = 40$ MeV, since such high energies are irrelevant for TGFs, to our knowledge.

235   To generate a simulated ASIM spectrum we proceeded to forward modeling of the

236   recorded spectrum, using a two stage simulation. In the first stage, a TGF is started at

237   12 km altitude, assuming one of the initial energy spectrums models, and is propagated

238   to the ISS altitude using the Geant4-based Monte-Carlo model presented in Sarria et al.

239   (2019) and publicly available (see acknowledgments). Energy, 3D-momentum, and times

240   of electrons/positrons reaching the ISS within a radius of 80 km (at ISS altitude) are saved.

241   At the end of this stage, at least 1 million particle records are required for each tested

242   source TGF spectrum model.

243   In the second stage, the recorded electrons/positrons are used as input of the ASIM

244   mass model to simulate the response of the instrument. It includes a local geomagnetic

245   field, and a rotation of frame of reference (Earth to ISS) is applied. The used mass model

246   includes the ASIM detector (MXGS, MMIA), the instrument platform, as well as non-

247   negligible surrounding elements (e.g. the Columbus module). The energy deposition on

248   the detectors can be direct, i.e. electrons/positrons hitting directly a CZT or BGO crys-

249   tal, or indirect. In the indirect case, electrons/positrons emit bremsstrahlung photons

250   by interaction with the surrounding material that hit at least one crystal. Photons can

251   also come from annihilating positrons, with specific energy of 511 keV. For HED, because

252   of the shielding, about 98 % of the energy deposition is due to indirect hits into the BGO

253   crystals. For LED, direct hits are more important: about 72 % of the energy deposition.

254   This explains why the effective area of LED is larger than HED when considering inci-

255   dent electrons/positrons. The effective area is calculated as the geometrical area (≈ 900

256   cm^2 for HED and $\approx 1024 \text{ cm}^2$ for LED) multiplied by the probability of an incident TEB

257   electron to deposit more than 300 keV into at least one BGO crystal (for HED), or more

258   than 50 keV into at least one CZT pixel (for LED).

259   At the end of the second stage, a simulation data set in the form of a list of detected

260   time and energy counts is generated. To be able to completely neglect the simulation noise,

261   it is required to have at least 1,000,000 counts on each detector to build each energy spec-

262   trum and calculate the effective areas. The final modeled spectrums also include a back-

263   ground component build from real background data.

264   A key feature of performing spectral analysis on the TEB, instead of TGF, is that

265   the energy spectrum (of secondary electrons and positrons) above 100 km altitude is only

266   weakly dependent on the following parameters:

267   • the radial distance between the TEB center and the ISS. The concept of radial

268   is presented more precisely in the supporting information, figure 1.

269   • the beaming and the tilt angles of the source TGF.

270   • the source altitude of the TGF, if set between 10 and 15 km.

271   Since these are crucial points for this analysis, we provide, in the supporting in-

272 formation document more detailed arguments and simulation results supporting those

273 three points. They permit a substantial simplification of the problem as it reduces dras-

274 tically the number of free parameters to include in the analysis. Actually, we found that

275 only the spectrum of the source TGF significantly affects the spectrum of the detected

276 TEB.

277   The simulated spectrums are evaluated with respect to the observation, separately

278 for the LED (50 to 370 keV) and the HED (0.3 to 40 MeV), and with both detectors to-

279 gether. To compare the modeling results to the observation, we use a likelihood anal-

280 ysis as well, a χ^2 analysis (Eadie et al., 1971; Martin, 1971; Lyons, 1986), as well as the

281 effective area ratio.

282   For the likelihood analysis, a value of $-2\,ln(\mathcal{L})$, the Negative Log-Likelihood, is cal-

283 culated. The model with the lowest value of $-2\,ln(\mathcal{L})$ is considered being the best de-

284 scription of the observation. Models are considered to be also possible if their $-2\,ln(\mathcal{L})$

285 values have a difference that is less than a threshold value τ. We calculated that $\tau \approx$

286 5 for a confidence level of about 99%, similar to the one used by Mailyan et al. (2016)

287 for Fermi-GBM observations. This value assumes that $-2\,ln(\mathcal{L})$ evolves following approx-

288 imately a normal (a.k.a. Gaussian) distribution with respect to the free parameter(s).

289 In the following, we present the values Δ_{mle}, that are the values of $-2\,ln(\mathcal{L})$ subtracted

290 by the value of $-2\,ln(\mathcal{L})$ for the best model. Therefore the best model has $\Delta_{mle} = 0$

291 and compatible models have $\Delta_{mle} \leq \tau$. A verification if a given model was found not

292 better than another just because of random fluctuations ("by chance") is also performed.

293   For completeness, we also provide a reduced χ^2 value, noted χ_r^2. If χ_r^2 is below a

294 critical value, the model is considered compatible with the measurement, and above the

295 model is considered incompatible. The Pearson χ^2 method is affected by choice of bin-

296 ning (i.e. energy intervals chosen to built the spectrums). To mitigate this effect, we chose

297 a binning with at least 7 measurement counts on each bin for HED, and at least 10 for

298 LED. These two binnings are used to make the spectrums presented in figure 2.b. Given

299 the used binning, the critical value $\chi^2_{r,c}$ is 1.94 (8 degrees of freedom) for LED, 1.75 for

300 HED (12 degrees of freedom) and 1.57 for the combination of both (20 degrees of free-

301 dom).

302 Compared to the Pearson's χ^2, the maximum likelihood analysis presents the ad-

303 vantage of not relying on a bining of the measurement data: it keeps all its granularity,

304 i.e. no information is lost by binning the measurements. The maximum likelihood anal-

305 ysis is better suited than the χ^2 to estimate which model is the best description of the

306 observation (see, for example, Hauschild and Jentschel (2001))

5 Results and discussion

308 Table 1 summarizes the results of this study. The models are sorted according the

309 prevalence of high energies (also called "hardness") or, equivalently, by decreasing LED/HED

310 effective area ratio. As indicated in the previous section, three main evaluation criteria

311 are presented: the reduced the Pearson's χ^2_r, the maximum likelihood, and the LED/HED

312 effective area ratio.

313 Concerning the LED spectral fits (table 1), all the models give good fits, using the

314 χ^2_r or the Maximum likelihood analysis. We interpret this as the energy range of 50 keV

315 to 370 keV being too narrow to discriminate between the models. Concerning the HED

316 spectral fits, looking at the χ^2_r values, only the 160 MV leader model is found incompat-

317 ible. This criteria gives similar conclusions when LED and HED spectrums are combined.

318 The maximum likelihood analysis on the HED spectrum indicates that the best model

319 is for $\epsilon = 8$ MeV. The fit for $\epsilon = 7.3$ MeV is also very close. It indicates that the leader

320 300 MV model and harder spectrums are also possible explanations. If LED and HED

321 spectrums are combined, the best model is then $\epsilon = 10$ MeV (but $\epsilon = 8$ MeV is a very

322 close fit here as well), and only models with $\epsilon = 6.5$ MeV or greater are compatible.

323 Since 307 counts are observed for LED (> 50 keV) and 168 for HED (> 300 keV),

324 the observed ratio is 1.83. Considering that the two count numbers individually follow

325 a Poisson statistic (but the ratio does not), the uncertainty on the ratio is ± 0.35 (95%

326 interval). It implies that, using this criteria, the two leader-based source TGF spectral

327 models (160 MV and 300 MV) are incompatible. The effective area ratio analysis indi-

328 cates that the models with $\epsilon \geq 6.5$ MeV are compatible. In particular we cannot ex-

329 clude $\epsilon = 8$ and $\epsilon = 10$ MeV. A similar conclusion is obtained with the maximum like-

330 lihood analysis (see last paragraph).

331 These results point towards TGF spectrums harder than previously expected. AG-

332 ILE did report observations of TGF surprisingly hard (up to 100 MeV), but they were

333 later found explainable from instrumental effects (Marisaldi et al., 2019). It does not ex-

334 clude that the mechanism presented in (Celestin et al., 2012), used first to explain TGF

335 spectrums up to 100 MeV, could not be responsible for producing TGFs with a bit harder

336 energy spectrums than typical RREA.

337 The results presented in this article are also only valid for a single event, and it does

338 not imply that leader models with potentials of 300 MV or less could explain other TGF

339 (and TEB) events. It is also possible that because our method relies on the detection

340 of a TEB, we are biased towards a population of strong TGFs, necessitating fully-developed

341 RREAs. TGFs that could originate from non-fully-developed RREAs (leader models)

342 may never (or very rarely) produce a detectable TEB. This question could be address-

343 able in the future, by applying this analysis to more TEB events. We list possibilities

344 of new studies in the next section.

345 Finally, table 1 also indicates the positron/electron ratio. The model giving the best

346 fit ($\epsilon = 10$ MeV) gives a ratio of 18.3%, and the range of compatible models give a ra-

347 tio ranging from 15.2% to 18.3%. This range is compatible with estimations from the

348 Fermi space telescope team (Briggs et al., 2011).

6 Conclusions and future work

349

350 We reported the observation of a Terrestrial Electron Beam by ASIM on March 24,

351 2019, originating from the rainbands of the tropical cyclone Johanina. The associated

352 lightining stroke was detected by the GLD360 network (VAISALA) in close temporal as-

353 sociation and very close to the ISS's south magnetic field line footpoint. The TEB spec-

354 trum was resolved down to 50 keV for the first time, using ASIM's low energy detector.

355 A method to constrain the TGF source energy spectrum based on the TEB detection

356 was presented. It relies on a key reduction of the number of free parameters (altitude,

357 angular distribution, radial distance) possible due to TEB's properties. Comprehensive

358 Monte-Carlo simulations were performed to reproduce the observation, assuming sev-

359 eral (energy) spectral shapes of the source TGF. Using three criteria to evaluate the sim-

ulation results with respect to the observation (Maximum likelihood, Pearson's χ_r^2 and LED/HED count ratio), we showed that source TGF with, at least, a fully-developed RREA spectrum $\propto E^{-1} \exp(-E/\epsilon)$ (with $\epsilon \geq 6.5$ MeV, $E_m = 40$ MeV) is compatible with the observation. We could not exclude harder models with $\epsilon = 8$ MeV ($E_m = 40$ MeV) and 10 MeV ($E_m = 40$ MeV), that could potentially be explained by non-equilibrium acceleration of energetic electrons in lightning (Celestin et al., 2012).

In the future, we expect that a larger number of events will be processed using the method presented in this article. For ASIM, it will not be possible before several more years of data gathering, since it currently detects about 4 TEB a year, and not all of them present LED data (only turned ON during ISS's night time) or enough counts on LED and HED. In principle, the method presented in this article could also be applied/translated to events from the Fermi GBM TGF/TEB catalog (Roberts et al., 2018), that currently contains about 30 TEB events. Fermi GBM has and high energy (BGO-based) detectors that covers an energy range of ≈ 150 keV to ≈ 30 MeV. GBM's NaI detectors could also be used in principle (with an energy range of a few keV to 1 MeV) but no TEB spectrum using it was reported yet. Since TEB events present lower fluxes (counts per second) than TGFs (typically 20 times), it makes the spectral analysis much less challenging than for TGF events. Instrumental effects (dead-time, pile-up), affecting TGF analysis, can be mostly (if not totally) ignored for TEB spectral analysis. In addition to Fermi, the method presented in this article could also be applied/translated to events from the TARANIS spacecraft, expected to launch at the end of 2020. TARANIS is equiped with detectors specifically designed for high energy photons as well as electrons (Lefeuvre et al., 2009; Sarria et al., 2017), and could potentially lead to an even more constrained analysis.

7 Acknowledgments

Model	Effective area in cm²		Effective area ratio	Maximum likelihood analysis result Δ_{mle}			Pearson's χ_r^2			e^+/e^- ratio
	LED	HED		LED	HED	Co.	LED	HED	Co.	
"Leader 160 MV" $\varepsilon = 4.3\,\text{MeV}$ $E_m = 19.2\ \text{MeV}$	122.0	43.7	2.79	**0**	19.0	22.5	**0.84**	1.97	1.66	10.3 %
"Leader 300 MV" $\varepsilon = 4.7\,\text{MeV}$ $E_m = 32\ \text{MeV}$	141.5	61.0	2.32	**0**	**3.4**	7.1	**0.88**	**1.04**	**1.31**	13.3 %
$\varepsilon = 6.5\,\text{MeV}$ $E_m = 40\ \text{MeV}$	156.0	74.4	**2.10**	**0.2**	**0.8**	**3.1**	**0.89**	**0.87**	**1.27**	15.2 %
$\varepsilon = 7.3\,\text{MeV}$ $E_m = 40\ \text{MeV}$	162.2	80.4	**2.02**	**0.3**	**0.2**	**1.9**	**0.88**	**0.85**	**1.28**	16.1 %
$\varepsilon = 8\,\text{MeV}$ $E_m = 40\ \text{MeV}$	168.4	85.5	**1.97**	**0.5**	**0**	**1.1**	**0.89**	**0.84**	**1.29**	16.8 %
$\varepsilon = 10\,\text{MeV}$ $E_m = 40\ \text{MeV}$	177.8	94.7	**1.88**	**0.5**	**1.0**	**0**	**0.90**	**0.83**	**1.30**	18.3 %
Compatibility range	n.a.		1.82±0.35	≤ 5			≤ 1.94	≤ 1.75	≤ 1.57	n.a.

Table 1. Table summarizing the comparison of the tested spectral models with the measurement. Three main criteria are presented: the LED/HED effective area ratio, the maximum likelihood and the Pearson's χ_r^2. "Co." stands for the LED and HED combination. The compatibility range for the different criteria are also indicated. Bold values indicate compatible models for the given criteria (column).
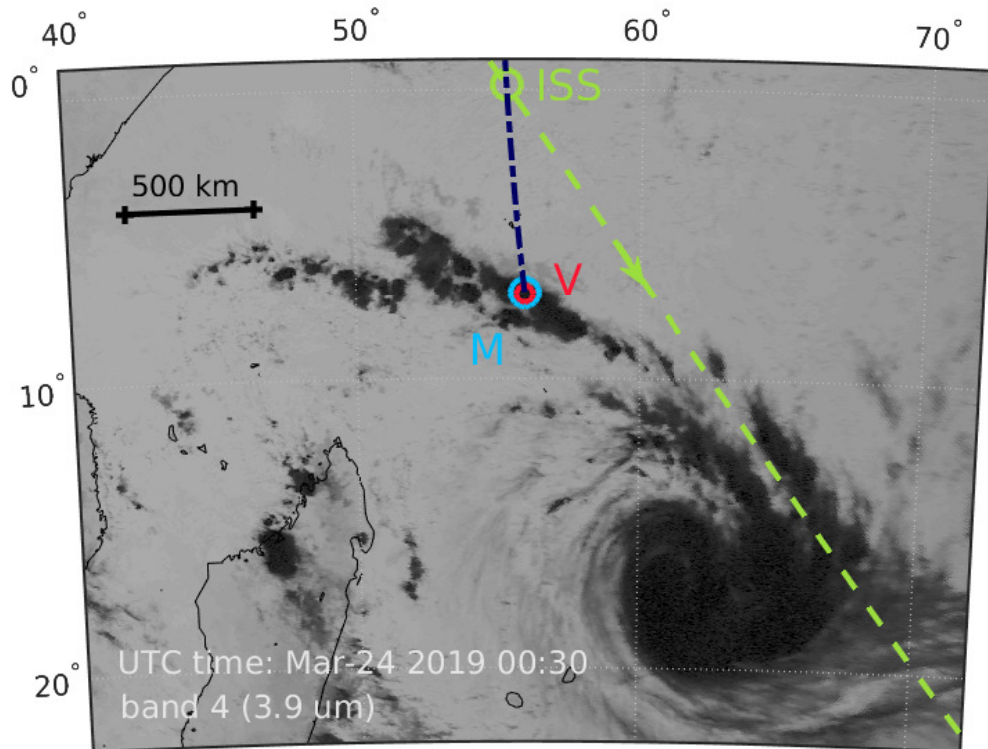
Figure 1. Image from geostationary satellite Meteosat-11 around 00:30 UTC, about 1 minute and 53 seconds before the ASIM trigger. The image comes from the optical band 4 (3.9 μm, 3 km resolution). The tropical cyclone Joaninha can be seen in the south-est part of the picture and extends over a thousand of kilometers. The positions of the International Space Station (ISS), the GLD360 match (V), and the magnetic field line footpoint (M) are indicated. The track of the Earth's magnetic field line (blue dashed line) and of of ISS trajectory (green dashed line) are also showed. Point V is very close to M in both location ($\Delta r = 4.82$ km) and time ($\Delta t = 1.44$ ms), and is located in the north-western rainbands of the cyclone.
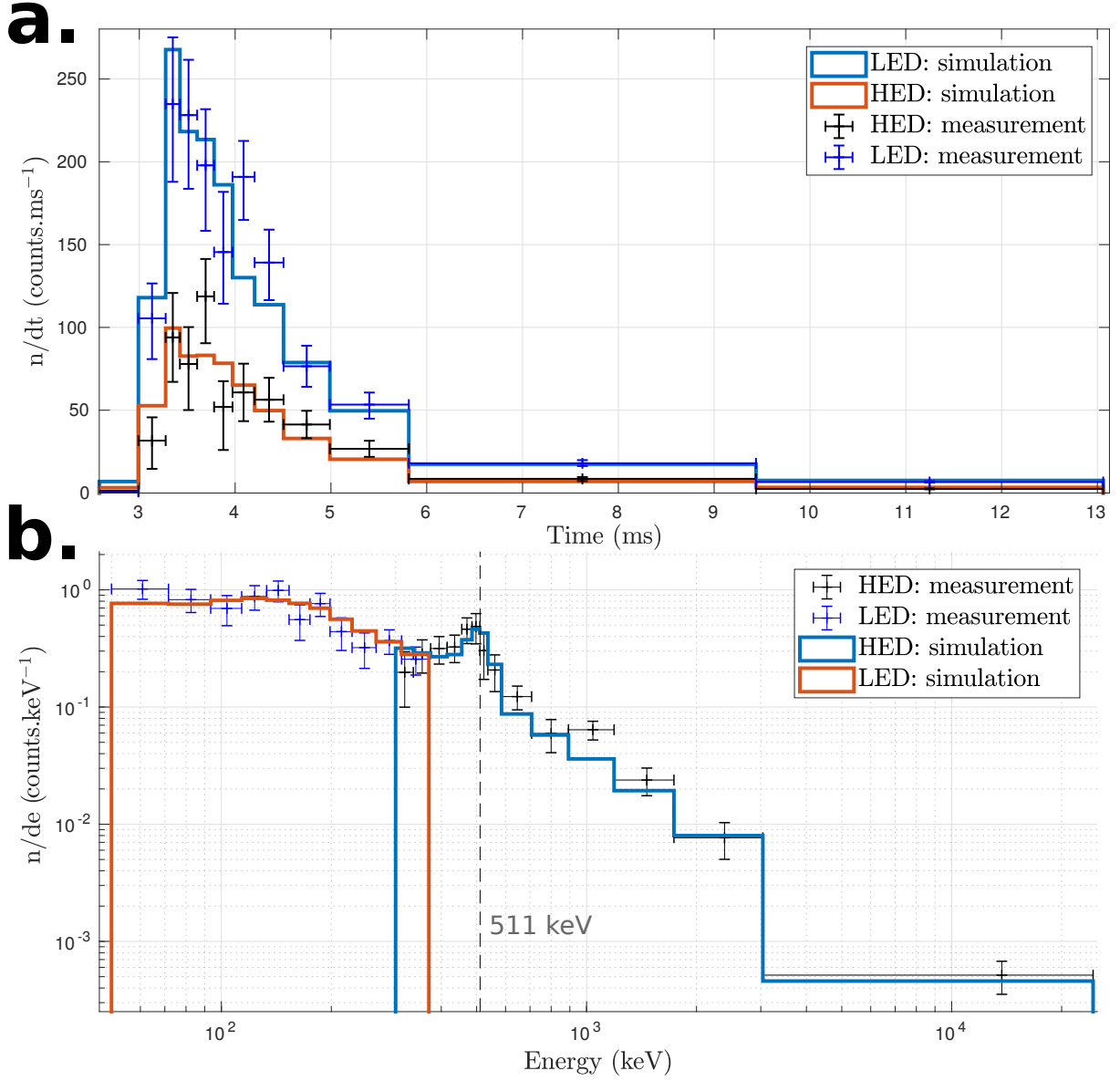
Figure 2. ASIM TEB event 190324. **a.** Recorded lightcurve by HED and LED, with 1-σ Poisson error bars. Simulation results from the consensus model are shown and give a good fit to the data ($\chi_r^2(\text{LED})_t = 1.33$, $\chi_r^2(\text{HED})_t = 1.34$). **b.** Recorded energy spectrum by HED and LED, with 1-σ Poisson error bars. Simulation results from the consensus model are shown and give a good fit to the data ($\chi_r^2(\text{LED})_e = 0.88$, $\chi_r^2(\text{HED})_e = 0.85$).

References

Babich, L. P., Donskoy, E. N., Kutsyk, I. M., & Roussel-Duprĕ, R. A. (2005). The feedback mechanism of runaway air breakdown. *Geophysical Research Letters*, *32*(9). Retrieved from `https://agupubs.onlinelibrary.wiley.com/doi/abs/10.1029/2004GL021744` doi: 10.1029/2004GL021744

Bowers, G. S., Smith, D. M., Martinez-McKinney, G., Kamogawa, M., Cummer, S., Dwyer, J., ... Kawasaki, Z. (2017). Gamma-ray signatures of neutrons from a terrestrial gamma-ray flash. *Geophysical Research Letters*.

Briggs, M. S., Connaughton, V., Wilson-Hodge, C., Preece, R. D., Fishman, G. J., Kippen, R. M., ... Smith, D. M. (2011, January). Electron-positron beams from terrestrial lightning observed with Fermi GBM. *Geophys. Res. Lett.*, *38*, L02808. doi: 10.1029/2010GL046259

Briggs, M. S., Fishman, G. J., Connaughton, V., Bhat, P. N., Paciesas, W. S., Preece, R. D., ... Chekhtman, A. (2010, July). First results on terrestrial gamma ray flashes from the Fermi Gamma-ray Burst Monitor. *Journal of Geophysical Research (Space Physics)*, *115*, A07323. doi: 10.1029/2009JA015242

Celestin, S., & Pasko, V. P. (2011, March). Energy and fluxes of thermal runaway electrons produced by exponential growth of streamers during the stepping of lightning leaders and in transient luminous events. *Journal of Geophysical Research (Space Physics)*, *116*, A03315. doi: 10.1029/2010JA016260

Celestin, S., Xu, W., & Pasko, V. P. (2012). Terrestrial gamma ray flashes with energies up to 100 mev produced by nonequilibrium acceleration of electrons in lightning. *Journal of Geophysical Research: Space Physics*, *117*(A5). Retrieved from https://agupubs.onlinelibrary.wiley.com/doi/abs/10.1029/2012JA017535 doi: 10.1029/2012JA017535

Celestin, S., Xu, W., & Pasko, V. P. (2015). Variability in fluence and spectrum of high-energy photon bursts produced by lightning leaders. *Journal of Geophysical Research: Space Physics*, *120*(12), 10,712-10,723. Retrieved from https://agupubs.onlinelibrary.wiley.com/doi/abs/10.1002/2015JA021410 doi: 10.1002/2015JA021410

Chanrion, O., Bonaventura, Z., Çinar, D., Bourdon, A., & Neubert, T. (2014, May). Runaway electrons from a 'beam-bulk' model of streamer: application to TGFs. *Environmental Research Letters*, *9*(5), 055003. doi: 10.1088/1748-9326/9/5/055003

Chanrion, O., Neubert, T., Lundgaard Rasmussen, I., Stoltze, C., Tcherniak, D., Jessen, N. C., ... Lorenzen, M. (2019, June). The Modular Multispectral Imaging Array (MMIA) of the ASIM Payload on the International Space Station. *Space Sci. Rev.*, *215*, 28. doi: 10.1007/s11214-019-0593-y

Cohen, M. B., Inan, U. S., Said, R. K., Briggs, M. S., Fishman, G. J., Connaughton, V., & Cummer, S. A. (2010, Sep). A lightning discharge producing a beam of relativistic electrons into space. Geophys. Res. Lett., *37*(18), L18806. doi: 10.1029/2010GL044481

Dwyer, J. R. (2008). Source mechanisms of terrestrial gamma-ray flashes. *Journal of Geophysical Research: Atmospheres*, *113*(D10), n/a–n/a. Retrieved from http://dx.doi.org/10.1029/2007JD009248 (D10103) doi: 10.1029/2007JD009248

Dwyer, J. R. (2012, February). The relativistic feedback discharge model of terrestrial gamma ray flashes. *J. Geophys. Res. (Space Phys)*, *117*(A2), A02308. doi: 10.1029/2011JA017160

Dwyer, J. R., Grefenstette, B. W., & Smith, D. M. (2008, January). High-energy electron beams launched into space by thunderstorms. Geophys. Res. Lett., *35*, L02815. doi: 10.1029/2007GL032430

Dwyer, J. R., Rassoul, H. K., Al-Dayeh, M., Caraway, L., Chrest, A., Wright, B., ... Rambo, K. J. (2005, January). X-ray bursts associated with leader steps in cloud-to-ground lightning. Geophys. Res. Lett., *32*, L01803. doi: 10.1029/2004GL021782

Dwyer, J. R., Rassoul, H. K., Al-Dayeh, M., Caraway, L., Wright, B., Chrest, A., ... Smyth, C. (2004, March). Measurements of x-ray emission from rocket-triggered lightning. Geophys. Res. Lett., *31*, L05118. doi: 10.1029/2003GL018770

Dwyer, J. R., Schaal, M., Rassoul, H. K., Uman, M. A., Jordan, D. M., & Hill, D. (2011, October). High-speed X-ray images of triggered lightning dart leaders. *Journal of Geophysical Research (Atmospheres)*, *116*, D20208. doi: 10.1029/2011JD015973

Dwyer, J. R., Smith, D. M., & Cummer, S. A. (2012, November). High-Energy Atmospheric Physics: Terrestrial Gamma-Ray Flashes and Related Phenomena. Space Sci. Rev., *173*, 133-196. doi: 10.1007/s11214-012-9894-0

Dwyer, J. R., Uman, M. A., Rassoul, H. K., Al-Dayeh, M., Caraway, L., Jerauld, J., ... Wright, B. (2003, January). Energetic Radiation Produced During Rocket-Triggered Lightning. *Science*, *299*, 694-697. doi: 10.1126/science.1078940

Eadie, W. T., Drijard, D., James, F. E., Roos, M., & Sadoulet, B. (1971). *Statistical*

methods in experimental physics. Amsterdam: North-Holland. Retrieved from
https://cds.cern.ch/record/100342

Fishman, G. J., Bhat, P., Mallozzi, R., Horack, J., Koshut, T., Kouveliotou, C., ...
others (1994). Discovery of intense gamma-ray flashes of atmospheric origin.
*Science-AAAS-Weekly Paper Edition-including Guide to Scientific Informa-
tion*, *264*(5163), 1313–1316.

Gjesteland, T. (2012). *Properties of Terrestrial Gamma ray Flashes. Modelling and
Analysis of BATSE and RHESSI data* (Doctoral dissertation, The University
of Bergen). Retrieved from http://bora.uib.no/handle/1956/6203

Gurevich, A. (1961). On the theory of runaway electrons. *Sov. Phys. JETP*, *12*(5),
904–912.

Gurevich, A., Milikh, G., & Roussel-Dupre, R. (1992). Runaway electron mechanism
of air breakdown and preconditioning during a thunderstorm. *Physics Letters
A*, *165*(5-6), 463–468.

Hauschild, T., & Jentschel, M. (2001). Comparison of maximum likelihood estima-
tion and chi-square statistics applied to counting experiments. *Nuclear Instru-
ments and Methods in Physics Research Section A: Accelerators, Spectrome-
ters, Detectors and Associated Equipment*, *457*(1), 384 - 401. Retrieved from
http://www.sciencedirect.com/science/article/pii/S0168900200007567
doi: https://doi.org/10.1016/S0168-9002(00)00756-7

Kohn, C., & Ebert, U. (2015). Calculation of beams of positrons, neutrons, and
protons associated with terrestrial gamma ray flashes. *Journal of Geophysical
Research: Atmospheres*, *120*(4), 1620-1635. Retrieved from https://agupubs
.onlinelibrary.wiley.com/doi/abs/10.1002/2014JD022229 doi: 10.1002/
2014JD022229

Lefeuvre, F., Blanc, E., & Pinçon, J. L. (2009, April). TARANIS-a Satellite Project
Dedicated to the Physics of TLEs and TGFs. In *American institute of physics
conference series* (Vol. 1118, p. 3-7). doi: 10.1063/1.3137711

Lindanger, A., Marisaldi, M., Maiorana, C., Sarria, D., Albrechtsen, K., Østgaard,
N., ... Verrecchia, F. (2020). The 3rd agile terrestrial gamma ray flash
catalog. part i: Association to lightning sferics. *Journal of Geophysical Re-
search: Atmospheres*, *125*(11), e2019JD031985. Retrieved from https://
agupubs.onlinelibrary.wiley.com/doi/abs/10.1029/2019JD031985

521   (e2019JD031985 10.1029/2019JD031985) doi: 10.1029/2019JD031985

522   Lyons, L. (1986). *STATISTICS FOR NUCLEAR AND PARTICLE PHYSICISTS.*

523   Mailyan, B. G., Briggs, M. S., Cramer, E. S., Fitzpatrick, G., Roberts, O. J., Stan-
524   bro, M., . . . Dwyer, J. R.   (2016, November).   The spectroscopy of individual
525   terrestrial gamma-ray flashes: Constraining the source properties.   *Journal of*
526   *Geophysical Research (Space Physics)*, *121*, 11. doi: 10.1002/2016JA022702

527   Mailyan, B. G., Xu, W., Celestin, S., Briggs, M. S., Dwyer, J. R., Cramer, E. S.,
528   . . . Stanbro, M.   (2019).   Analysis of individual terrestrial gamma-ray flashes
529   with lightning leader models and fermi gamma-ray burst monitor data.   *Jour-*
530   *nal of Geophysical Research: Space Physics*, *124*(8), 7170-7183.   Retrieved
531   from https://agupubs.onlinelibrary.wiley.com/doi/abs/10.1029/
532   2019JA026912   doi: 10.1029/2019JA026912

533   Marisaldi, M., Fuschino, F., Tavani, M., Dietrich, S., Price, C., Galli, M., . . . Vercel-
534   lone, S.   (2014, February).   Properties of terrestrial gamma ray flashes detected
535   by AGILE MCAL below 30 MeV.   *Journal of Geophysical Research (Space*
536   *Physics)*, *119*, 1337-1355. doi: 10.1002/2013JA019301

537   Marisaldi, M., Galli, M., Labanti, C., Østgaard, N., Sarria, D., Cummer, S. A.,
538   . . . Verrecchia, F.   (2019, Jul 27).   On the high-energy spectral compo-
539   nent and fine time structure of terrestrial gamma ray flashes.   *Journal of*
540   *Geophysical Research: Atmospheres*, *124*(14), 7484-7497.   Retrieved from
541   https://doi.org/10.1029/2019JD030554   doi: 10.1029/2019JD030554

542   Martin, B. R.   (1971).   *Statistics for physicists [by] b. r. martin* [Book].   Academic
543   Press London, New York.

544   Moss, G. D., Pasko, V. P., Liu, N., & Veronis, G.   (2006, February).   Monte Carlo
545   model for analysis of thermal runaway electrons in streamer tips in transient
546   luminous events and streamer zones of lightning leaders.   *Journal of Geophysi-*
547   *cal Research (Space Physics)*, *111*, 2307. doi: 10.1029/2005JA011350

548   Neubert, T., Østgaard, N., Reglero, V., Blanc, E., Chanrion, O., Oxborrow,
549   C. A., . . . Bhanderi, D. D. V.   (2019, Mar 12).   The ASIM Mission on
550   the International Space Station.   *Space Science Reviews*, *215*(2), 26.   Re-
551   trieved from https://doi.org/10.1007/s11214-019-0592-z   doi:
552   10.1007/s11214-019-0592-z

553   Neubert, T., Østgaard, N., Reglero, V., Chanrion, O., Heumesser, M., Dimitriadou,

554   K., . . . Eyles, C. J.   (2020, January).   A terrestrial gamma-ray flash and

555   ionospheric ultraviolet emissions powered by lightning.   *Science*, *367*(6474),

556   183-186. doi: 10.1126/science.aax3872

557 Østgaard, N., Balling, J. E., Bjørnsen, T., Brauer, P., Budtz-Jørgensen, C., Bu-

558   jwan, W., . . . Yang, S.   (2019, February).   The Modular X- and Gamma-Ray

559   Sensor (MXGS) of the ASIM Payload on the International Space Station.

560   Space Sci. Rev., *215*, 23. doi: 10.1007/s11214-018-0573-7

561 Østgaard, N., Neubert, T., Reglero, V., K., U., S., Y., G., G., . . . S., A.-N.   (2019).

562   First ten months of TGF observations by ASIM.   *Journal of Geophysical Re-*

563   *search (Atmospheres)*. (Submitted)

564 Roberts, O. J., Fitzpatrick, G., Stanbro, M., McBreen, S., Briggs, M. S., Holzworth,

565   R. H., . . . Mailyan, B. G.   (2018, May).   The First Fermi-GBM Terrestrial

566   Gamma Ray Flash Catalog.   *Journal of Geophysical Research (Space Physics)*,

567   *123*, 4381-4401. doi: 10.1029/2017JA024837

568 Sarria, D., Blelly, P.-L., & Forme, F.   (2015, May).   MC-PEPTITA: A Monte Carlo

569   model for Photon, Electron and Positron Tracking In Terrestrial Atmosphere.

570   Application for a terrestrial gamma ray flash.   *Journal of Geophysical Research*

571   *(Space Physics)*, *120*, 3970-3986. doi: 10.1002/2014JA020695

572 Sarria, D., Kochkin, P., Østgaard, N., Lehtinen, N., Mezentsev, A., Marisaldi, M.,

573   . . . Eyles, C. (2019, December). The First Terrestrial Electron Beam Observed

574   by the Atmosphere-Space Interactions Monitor.   *Journal of Geophysical Re-*

575   *search (Space Physics)*, *124*(12), 10,497-10,511. doi: 10.1029/2019JA027071

576 Sarria, D., Lebrun, F., Blelly, P.-L., Chipaux, R., Laurent, P., Sauvaud, J.-A., . . .

577   Lindsey-Clark, M.   (2017, July).   TARANIS XGRE and IDEE detection

578   capability of terrestrial gamma-ray flashes and associated electron beams.

579   *Geoscientific Instrumentation, Methods and Data Systems*, *6*, 239-256.   doi:

580   10.5194/gi-6-239-2017

581 Sarria, D., Rutjes, C., Diniz, G., Luque, A., Ihaddadene, K. M. A., Dwyer, J. R., . . .

582   Ebert, U. (2018, November). Evaluation of Monte Carlo tools for high-energy

583   atmospheric physics II: relativistic runaway electron avalanches.   *Geoscientific*

584   *Model Development*, *11*, 4515-4535. doi: 10.5194/gmd-11-4515-2018

585 Skeltved, A. B., Østgaard, N., Carlson, B., Gjesteland, T., & Celestin, S.   (2014,

586   November).   Modeling the relativistic runaway electron avalanche and the

feedback mechanism with GEANT4. *Journal of Geophysical Research (Space Physics)*, *119*, 9174-9191. doi: 10.1002/2014JA020504

Skeltved, A. B., Østgaard, N., Mezentsev, A., Lehtinen, N., & Carlson, B. (2017). Constraints to do realistic modeling of the electric field ahead of the tip of a lightning leader. *Journal of Geophysical Research: Atmospheres*, *122*(15), 8120-8134. Retrieved from `https://agupubs.onlinelibrary.wiley.com/doi/abs/10.1002/2016JD026206` doi: 10.1002/2016JD026206

Smith, D. M., Grefenstette, B. W., Splitt, M., Lazarus, S. M., Rassoul, H. K., Coleman, L. M., ... Takahashi, Y. (2006, December). The Anomalous Terrestrial Gamma-ray Flash of 17 January 2004. *AGU Fall Meeting Abstracts*, AE31A-1040.

Smith, D. M., Lopez, L. I., Lin, R. P., & Barrington-Leigh, C. P. (2005, February). Terrestrial Gamma-Ray Flashes Observed up to 20 MeV. *Science*, *307*, 1085-1088. doi: 10.1126/science.1107466

Ursi, A., Guidorzi, C., Marisaldi, M., Sarria, D., & Frontera, F. (2017, April). Terrestrial gamma-ray flashes in the BeppoSAX data archive. *Journal of Atmospheric and Solar-Terrestrial Physics*, *156*, 50-56. doi: 10.1016/j.jastp.2017.02.014

Wilson, C. T. R. (1924, January). The electric field of a thundercloud and some of its effects. *Proceedings of the Physical Society of London*, *37*, 32D-37D.

Xu, W., Celestin, S., Pasko, V. P., & Marshall, R. A. (2019). Compton scattering effects on the spectral and temporal properties of terrestrial gamma-ray flashes. *Journal of Geophysical Research: Space Physics*, *124*(8), 7220-7230. Retrieved from `https://agupubs.onlinelibrary.wiley.com/doi/abs/10.1029/2019JA026941` doi: 10.1029/2019JA026941